

pubs.acs.org/est Article

Removal of Aqueous Uranyl and Arsenate Mixtures after Reaction with Limestone, PO_4^{3-} , and Ca^{2+}

Isabel Meza, Han Hua,* Kaelin Gagnon, Anjali Mulchandani, Jorge Gonzalez-Estrella, Peter C. Burns, Abdul-Mehdi S. Ali, Michael Spilde, Eric Peterson, Peter Lichtner, and José M. Cerrato*



Cite This: Environ. Sci. Technol. 2023, 57, 20881-20892



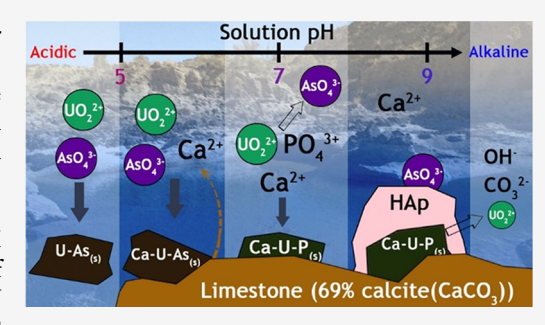
ACCESS

III Metrics & More

Article Recommendations

s Supporting Information

ABSTRACT: The co-occurrence of uranyl and arsenate in contaminated water caused by natural processes and mining is a concern for impacted communities, including in Native American lands in the U.S. Southwest. We investigated the simultaneous removal of aqueous uranyl and arsenate after the reaction with limestone and precipitated hydroxyapatite (HAp, $\text{Ca}_{10}(\text{PO}_4)_6(\text{OH})_2$). In benchtop experiments with an initial pH of 3.0 and initial concentrations of 1 mM U and As, uranyl and arsenate coprecipitated in the presence of 1 g L⁻¹ limestone. However, related experiments initiated under circumneutral pH conditions showed that uranyl and arsenate remained soluble. Upon addition of 1 mM PO₄³⁻ and 3 mM Ca²⁺ in solution (initial concentration of 0.05 mM U and As) resulted in the rapid removal of over 97% of U via Ca–U–P



precipitation. In experiments with 2 mM PO₄³⁻ and 10 mM Ca²⁺ at pH rising from 7.0 to 11.0, aqueous concentrations of As decreased (between 30 and 98%) circa pH 9. HAp precipitation in solids was confirmed by powder X-ray diffraction and scanning electron microscopy/energy dispersive X-ray. Electron microprobe analysis indicated U was coprecipitated with Ca and P, while As was mainly immobilized through HAp adsorption. The results indicate that natural materials, such as HAp and limestone, can effectively remove uranyl and arsenate mixtures.

KEYWORDS: uranium, arsenic, uranyl, arsenate, hydroxyapatite, limestone, precipitation, adsorption

■ INTRODUCTION

Co-occurrence of U (uranyl) and As (arsenate) mixtures in contaminated waters has been reported in several sites affected by mining legacy in the Southwestern U.S. $^{1-3}$ Much of the mining activity occurred on Native American lands and has left a lasting legacy of contamination. In the Navajo Nation alone, there are more than 500 abandoned uranium mine sites, remediation of which will cost billions of dollars. Previous studies have shown that waters on Southwest Native American lands were impacted by associated anthropogenic activities and natural processes. Incidents of uranium contamination were detected at levels 20 times higher than the maximum concentration limit (MCL) of 30 μ g L U set by the U.S. Environmental Protection Agency (EPA) for drinking water, while As concentrations were more than 3 times that of the EPA MCL (10 μ g L As).

The mobility of both uranyl, $(\mathrm{UO_2})^{2^+}$, and arsenate, $\mathrm{AsO_4}^{3^-}$, in oxic conditions is a function of environmental factors including pH, $^{19-22}$ complexation chemistry, $^{23-27}$ and soil/mineral interactions. $^{28-31}$ The uranyl $(\mathrm{UO_2})^{2^+}$ ion is the dominant aqueous species under acidic conditions (pH < 5), and their co-occurrence with arsenates has been reported as the meta-autunite group $(\mathrm{A^{n+}[(\mathrm{UO_2})(\mathrm{TO_4})]}\ (\mathrm{H_2O}))$, where $\mathrm{A^{n+}}$ is a mono-, di-, or trivalent cation and T = P or As). 32 At circumneutral and alkaline conditions, anionic aqueous

complexes can form after the reaction of uranyl with carbonate, hydroxide, or phosphate, among other ligands.^{33–36} Critical complexation reactions with cations also control the precipitation and dissolution of U contaminants. Our previous study reported that dissolution of uranyl arsenate solids is enhanced by complexing with Ca²⁺ and (bi)carbonate at pH 7 via the formation of Ca-U(VI)-CO₃ ternary complexes. 18 Precipitates of NaUAs(s) and KUAs(s) were found to have 3 orders of magnitude faster dissolution rate constants than uranyl phosphate analogues minerals at pH 2.37 In natural conditions, Ca-U-As bearing solids occurs as uranospinitelike secondary uranium minerals, for example, zeunerite $[Cu(UO_2)_2(AsO_4)_2 \cdot H_2O]$, walpurgite $[(BiO)_4(UO_2)(AsO_4)_2 \cdot H_2O]$ $2H_2O$], and trögerite $[(H_3O)(UO_2)(AsO_4)\cdot 3H_2O]$. The surface charges on natural minerals also affect the adsorption of $(UO_2)^{2+}$ ions. For example, quartz, albite, and calcite exhibit positive surface charges at acidic conditions. ^{40–42} Applying a PO₄³⁻ supplement along with Ca²⁺ to immobilize uranyl in

Received: May 19, 2023 Revised: November 6, 2023 Accepted: November 7, 2023 Published: November 29, 2023





Table 1. Initial Conditions for Different Experiments Conducted in This Study

experimental sets	arsenate and uranyl source	initial pH	limestone (g L ⁻¹)	PO ₄ ³⁻ (mM)	Ca ²⁺ (mM)	As(V) (arsenate) (mM)	U(VI) (uranyl) (mM)
(1) U-As-L (with limestone)	$\begin{bmatrix} Na_2HAsO_4\cdot7H_2O \end{bmatrix}, \\ \begin{bmatrix} UO_2(CH_3CO_2)_2\cdot2H_2O \end{bmatrix}$	3.0 and 7.0	1	0	0	1	1
(2) U-As-Ca-PO ₄ -L	(As_2O_5) , $[UO_2(NO_3)2.6H_2O]$	3.0 and 7.0	1	1	3	0.05	0.05
(3) U-As (no limestone)	$\begin{bmatrix} Na_2HAsO_4\cdot7H_2O \end{bmatrix}, \\ \begin{bmatrix} UO_2(CH_3CO_2)_2\cdot2H_2O \end{bmatrix}$	3.0 and 7.0	0	0	0	1	1
(4) U-As-Ca-PO ₄	(As_2O_5) , $[UO_2(NO_3)2.6H_2O]$	3.0 and 7.0	0	1	3	0.05	0.05
(5) U-As-Ca-PO ₄ (HAp)	$(As_2O_5), [UO_2(NO_3)2.6H_2O]$	between 5.0 and 7.0	0	2	10	0.05	0.05
(6) U-As-Ca-PO ₄ -L (limestone + HAp)	(As_2O_5) , $[UO_2(NO_3)2\cdot 6H_2O]$	between 5.0 and 7.0	1	2	10	0.05	0.05

water has been studied based on mechanisms of uranyl adsorption onto Ca-P solids, Ca-U-P coprecipitation, and uranyl incorporation depending on the pH and orders of reactant addition. However, the presence of PO₄³⁻ can result in the dissolution of arsenate, for the competitive ion displacement between AsO₄³⁻ and PO₄³⁻ in complexation reactions with U.^{17,48,49} Designing a process that can remove uranyl and arsenate simultaneously in contaminated waters is challenging, given that the attenuation of uranium would have to be accomplished without triggering the release of arsenic and vice versa. This challenge of enabling the removal of uranyl and arsenate with reactants that could be accessible to underserved communities serves as the motivation for this study.

Limestone is an abundant sedimentary rock in the vicinity of sandstone-hosted uranium deposits in geologic formations, such as the Jackpile Mine in New Mexico where U and As cooccur.³⁴ Limestone mainly consists of calcite (CaCO₃) and various trace metal impurities, such as iron, aluminum, sodium, and potassium, as well as detrital minerals, including quartz. 50,51 Natural limestone has been utilized for the removal of heavy metals like Pb(II), Cd(II), Cu(II), and Zn(II) from solutions through sorption reactions, owing to its economic feasibility. 52-54 Previous studies reported that calcite can uptake arsenate anions via surface complexation. 55,56 The sorption behavior is considered to be influenced by competition for sorption sites with (bi)carbonate, protonation/deprotonation of the arsenate ion, and ionic strength of the solution. Nevertheless, the effectiveness of removal may be diminished by characteristics of natural limestone, including mineral components, particle size, surface charge, and trace elements incorporated at grain boundaries. 54,57

Hydroxyapatite (HAp, Ca₁₀(PO₄)₆(OH)₂) is a well-studied mineral adsorbent for removing metal contaminants from water.⁵⁸ Apatite minerals are found in igneous rocks such as pegmatites,⁵⁹ and the natural formation of HAp is more commonly observed through biological pathways.⁶⁰ Chemical precipitation can also be used to synthesize HAp, but the structural Ca and P stoichiometry and byproducts such as dicalcium phosphate dihydrate (brushite, CaHPO₄·2H₂O) and octacalcium phosphate (Ca₈H₂(PO₄)6·5H₂O) are influenced by solution pH, temperature, and reaction rates. 61,62 HAp has been applied in the removal of both U and As through mechanisms such as electrostatic attraction and dissolutionprecipitation. 63-65 Other studies have reported HAp coatings were utilized to enhance the reactivity of activated carbon, ^{66,6} minerals, ^{68–70} polymeric materials, ⁷¹ and biotic materials ^{72–7} for removal reactions. However, further investigations are necessary to identify the key adsorption and precipitation removal mechanisms under both acidic and neutral pH

conditions for U and As mixtures using natural limestone with additions of Ca²⁺ and PO₄³.

In the present study, we investigated the removal of uranyl and arsenate mixtures from solutions by reaction with natural limestone as well as added Ca^{2+} and PO_4^{3-} . Bench experiments were performed at low and neutral initial pH (3.0 and 7.0, respectively) with 3 mM Ca²⁺ and 1 mM PO₄³⁻ to remove uranyl and arsenate mixtures in the presence and absence of limestone. Additional experiments were conducted with higher concentrations of Ca (10 mM Ca²⁺) and P (2 mM PO₄³⁻) to promote HAp precipitation with a pH increase from 7.0 to 11.0, which could improve arsenate removal. The novelty of this study is the use of natural materials, such as Ca²⁺, PO₄³⁻ hydroxyapatite, and limestone, for the removal of uranyl and arsenate mixtures from contaminated waters through adsorption and coprecipitation mechanisms. The experimental data and approach presented in this research provide a potential onsite remediation strategy to reduce environmental risks for communities exposed to U and As contamination in the Western U.S. and other parts of the world.

MATERIALS AND METHODS

Limestone Characterization. Limestone used in this study was collected from the Sandia Formation, Sandia Mountains, near Albuquerque, New Mexico. The specimen was crushed and sieved to obtain a surface area of ~2 m² g⁻¹ that has been measured by nitrogen (N2) absorptiometry (Micromeritics Gemini 2360 Brunauer, Emmett, and Teller Surface Area Analyzer)⁷⁵ after degasification [see sample preparation in the Supporting Information (SI), Text S1]. Zeta-potential data were acquired with a Malvern Zetasizer Nano-ZS equipped with a He-Ne laser (633 nm) and noninvasive backscatter optics. All samples were suspended at a 0.1 mg mL⁻¹ concentration. Measurements were acquired at 25 °C. The zeta potentials for all the samples were measured in triplicate according to the Smoluchowski theory. All reported values correspond to the average of three measurements of the collected sample. Moreover, single-step acid digestion with inductively coupled plasma optical emission spectroscopy (ICP-OES) and electron microprobe analysis (EMA) were applied to identify elemental concentrations in the limestone (see more details in the Supporting Information, Text S1).

Batch Experiments. The initial conditions used for batch experiments in this study are listed in Table 1. Briefly, experiments used the following initial conditions. (1) 1 mM aqueous arsenate and uranyl in solutions with 1 g L-1 limestone at initial pH 3.0 and 7.0; (2) 0.05 mM arsenate and uranyl in solutions with 1 mM PO₄³⁻, 3 mM Ca²⁺, and 1 g L^{-1} limestone [(Table 1, sets (1) and (2)]). The concentration

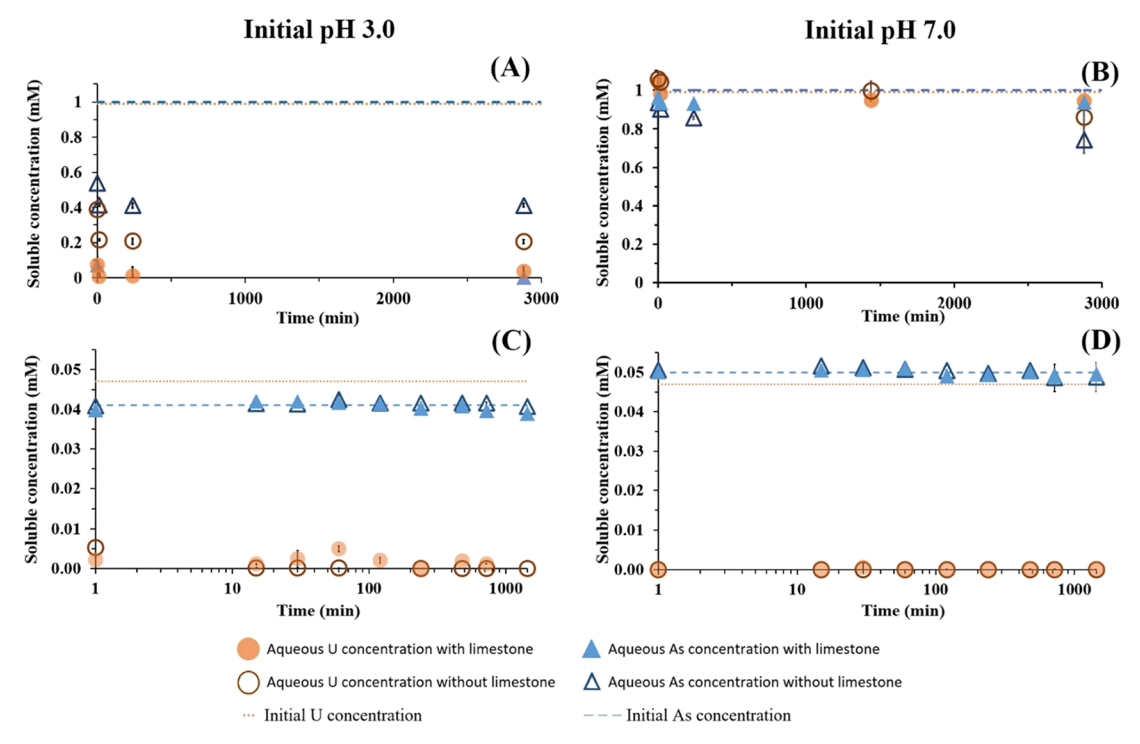


Figure 1. Concentrations of aqueous U(VI) and As(V) as a function of time: (A) experiments supplied with 1 mM of U and As with and without 1 g L^{-1} of limestone at initial pH 3.0; (B) experiments supplied with 1 mM of U and As with and without 1 g L^{-1} of limestone at initial pH 7.0; (C) experiments supplied with 0.05 mM of U and As, 1 mM of PO₄³⁻ and 3 mM of Ca²⁺ with and without 1 g L^{-1} of limestone at initial pH 3.0; and (D) experiments supplied with 0.05 mM of U and As, 1 mM of PO₄³⁻ and 3 mM of Ca²⁺ with and without 1 g L^{-1} of limestone at initial pH 7.0. Error bars represent the standard deviation of triplicate treatments.

of 3 mM Ca²⁺ is based on the range measured from 0.2 to 7 mM reported in Rio Paguate, New Mexico in a previous publication of our research group.³⁴ The concentration of 1 mM PO₄³⁻ was chosen based on other studies which report that at this level Ca-P can react to precipitate, and uranyl phosphate precipitation can occur. The solution's initial pH is set to 3.0 and 7.0 according to the acidic pH reported in groundwater 16,76,77 and at circumneutral pH reported in surface water in the proximity of sites affected by mining legacy.³⁴ Hydrochloric acid (HCl) and ammonium hydroxide (NH₄OH) are used for pH adjustment. For comparison purposes, parallel experiments were conducted without limestone [Table 1, sets (3) and (4)]. Mixed solutions were contained in triplicate 50 mL centrifuge tubes loaded on a tube rotator. A volume of 2.0 mL was taken for liquid samples at 0, 15, 1440, and 2880 min for sets (1) and (3), and 0, 15, 30, 60, 120, 480, 720, and 1440 min for sets (2) and (4). The elevated concentrations of 1.0 mM of aqueous arsenate and uranyl were chosen for these experiments to represent water contamination at ranges reported in the literature from hundreds to thousands of mg/L for environments impacted by natural and anthropogenic activities.^{78–81} The concentrations of 0.05 mM uranyl and arsenate were chosen for these experiments to represent concentration ranges that have been reported in waters affected by mining legacy. 2,16,34,82

In tripilicate experiments with increasing pH from 7.0 to 11.0 [Table 1, sets (5) and (6)], 200 mL of solutions included initially 10 mM Ca²⁺, 2 mM PO₄³⁻, 0.05 mM uranyl and arsenate with and without 1 g L⁻¹ limestone in glass beakers. Solution pH was continuously monitored throughout the experiments, as ammonium hydroxide was added drop by drop. A volume of 2.0 mL of liquid sample was taken after

shaking for 1 h (with an orbital shaker at 120 rpm), which was conducted when it reached pH 7.0, 8.0, 9.0, 10.0, and 11.0. The whole process took approximately 7 h.

Dissolved uranyl was supplied by uranyl acetate $[UO_2(CH_3CO_2)_2 \cdot 2H_2O]$ or uranyl nitrate $[UO_2(NO_3)_2 \cdot$ 6H2O], while arsenate was from sodium arsenate [Na₂HAsO₄·7H₂O] or arsenic pentoxide [As₂O₅]. Supplements of Ca²⁺ and PO₄³⁻ in solutions were provided by CaCl₂· 2H₂O and NH₆PO₄. Adjustment of solution pH was performed using HNO3 and NH4OH. More experimental information is detailed in the Supporting Information (Table S1). Water used in all experiments was from Ultrapure Water (18.2 M Ω) Systems. pH measurements were provided by benchtop Thermo Fisher pH meters, which were calibrated with standard buffer solutions at pH values of 5.0, 7.0, and 10.0 prior to the experiments. All experiments were conducted in an open atmosphere with a CO_2 partial pressure of $1 \times 10^{-3.5}$ bar. It was assumed that equilibrium between the solution and air CO2 would be reached through a shaking process lasting at least 1 h.

Liquid Analyses. Liquid samples were passed through 0.2 μ m membranes, acidified by the addition of 2% HNO₃ to pH around 2, and refrigerated at 4 °C prior to subsequent analyses. Concentrations of As, U, Ca, and P in solutions were quantified by ICP-OES and/or mass spectrometry (ICP-MS) (for metal concentrations lower than 1 mg/L). Concentrations of PO₄³⁻ were measured using an ion chromatography (IC) system. Supporting Information contains more details (Text S1).

Solid Analyses. Limestone and precipitates were collected after the experiments by centrifuging and air-drying in a laboratory hood. A set of analyses was applied to characterize

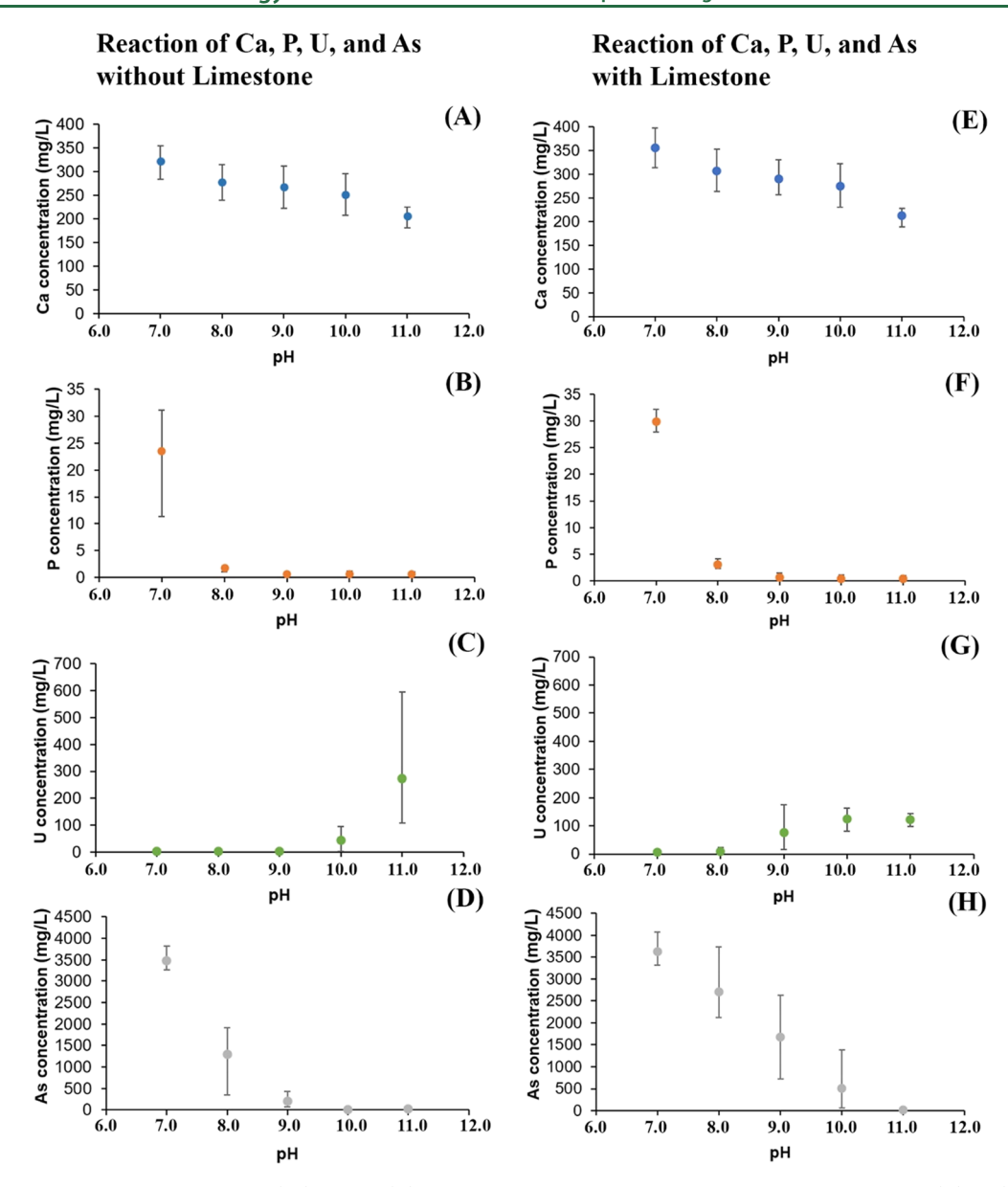


Figure 2. Concentrations of aqueous Ca, P, U(VI), and As(V) in solutions are plotted as a function of pH. Figures from (A) to (D) represent the experiment with initial concentrations of 10 mM Ca (400.8 mg/L), 2 mM P (61.9 mg/L), 0.05 mM As (3,746 µg/L), and 0.05 mM U (11,901 µg/L) L). Figures from (E) to (H) represent data of parallel sets with additional limestone of 1 g L⁻¹. Error bars represent the minimum and maximum values of triplicate treatments.

mineralogy, morphology, and surface elemental composition of limestone and precipitates, including using powder X-ray diffraction (pXRD), scanning electron microscopy (SEM) with energy dispersive X-ray (EDX) spectroscopy, and EMA with wavelength dispersive X-ray spectroscopy. See more details in Supporting Information (Text S1).

Chemical Speciation Calculations. Chemical speciation modeling was carried out using the open-source computer code PFLOTRAN that runs on MacOSX, linux and Windows.⁸³ Speciation calculations were based on chemical equilibrium modeling using inputs from experimental conditions used in this study as a tool to gain insight into aqueous complexation and the solid saturation state. PFLOTRAN can perform speciation calculations with options to input total and free ion concentrations, mineral and gas equilibrium constraints, pH, and charge balance. The extended Debye-Hückel algorithm is used to compute activity coefficients. The

PFLOTRAN thermodynamic database was expanded to include equilibrium constants at 25 °C for becquerelite taken from Gorman-Lewis et al.,84 and for uranyl arsenates from Nipruk et al. 84,85 and includes the most recent update to U complexes. 35,86–88 We used the unpublished constant for uranospinite $[Ca(UO_2)_2(AsO_4)_2]$ log $K_{sp} = -42.499$. The geochemical system was described with the following primary species: UO₂²⁺, AsO₄³⁻, Ca²⁺, Na⁺, H⁺, CO₃²⁻, NO₃⁻, NH₄⁺, PO₄³⁻, and Cl⁻. In the experiments, we assumed a partial pressure of CO₂ in equilibrium with the atmosphere of 10^{-3.5} bar (pCO₂ = 3.5).

RESULTS AND DISCUSSION

Limestone Characterization. Collected natural limestone mainly contains Ca (23.4 wt %), Mg (0.7 wt %), and Al (0.5 wt %) based on triplicate single-step acid digestion with ICP-OES analysis. Results are generally consistent with backscatter

electron image by EMA on natural limestone (Supporting Information, Table S2). Identification and Rietveld quantitative analyses with pXRD reveal that the limestone used in this study consists of calcite (CaCO₃, ~69 wt %) and quartz (SiO₂, ~26 wt %) (Supporting Information, Figure S1). Zetapotential analysis indicated that net charges of limestone surfaces were negative at pH ranging from 2 to 9 (Supporting Information, Figure S2). Although reported points of zero charge (PZC) for synthesized calcite were between pH 8 and 9,89,50 inconsistent PZC values have been reported in other studies on natural calcite and/or limestone. The inconsistency could be attributed to various elements and trace minerals in the limestone, and ion groups adsorbed on surfaces at natural conditions. 91 Another potential factor affecting the particle surface charges could be full oxidation during the limestone grinding process.

Aqueous Uranyl and Arsenate Removal Impacted by Ca^{2+} , PO_4^{3+} , and Limestone with Initial pH of 3.0 and 7.0. In solutions with initial concentrations of 1 mM uranyl and arsenate and an initial pH of 3.0 (Table1), ~80% of the aqueous uranyl and ~60% of the aqueous arsenate were removed without reaction with limestone, Ca^{2+} , and PO_4^{3+} (Figure 1A). After the addition of 1 g L^{-1} limestone, the solution pH was neutralized to between 5 and 7 (Supporting Information, Figures S3 and S4), and removals of ~96% of aqueous U, and ~100% As were observed (Figure 1A). In contrast, more than 86% of U and more than 74% of As remained soluble at circumneutral pH after 48 h (2880 min) in experiments without limestone at initial pH of 7.0 (Figure 1B).

The precipitation and stability of uranyl arsenate solids at acidic pH have been reported in other studies. For example, a previous study identified a solid similar to uranospinite $[Ca(UO_2)_2(AsO_4)_2\cdot 10H_2O]$ after the reaction of U, As, and Ca in water at pH 3. Other researchers reported the stability of uranyl arsenate solids at acidic pH after reaction with cations, such as Na⁺ and K⁺. S5,92 In contrast, the dissolution of U and As has been reported in experiments conducted at circumneutral pH due to the influence of uranyl carbonate aqueous complexes that contribute to the mobility of U and As. These findings from previous investigations are consistent with the observation of this study and the chemical speciation calculation by using PFLOTRAN (Supporting Information, Table S3 and Figure S5).

With the addition of 3 mM Ca²⁺ and 1 mM PO₄³⁻ [Table 1 sets (2) and (4)], more than 90% U removal was observed at both initial pH 3.0 and 7.0 (Figure 1C,D, respectively). Arsenate remained soluble due to the competitive replacement between (PO₄)³⁻ and (AsO₄)³⁻.⁴⁹ As illustrated in Table S3, the percentages of abundance of the chemical species of AsO₄³⁻ and PO₄³⁻ are similar due to their analogue oxyanion behavior and deprotonation. White Ca–P precipitates formed in solutions with Ca²⁺ and PO₄³⁻ supplements but did not result in improved arsenate removal after 24 h (1440 min). The potential enhancement from the presence of limestone was not distinguishable in solutions with the PO₄³⁻ supplements. A similar phenomenon was observed in experiments conducted at both initial pH 3.0 and 7.0.

Other studies have immobilized aqueous uranyl by adding Ca^{2+} and PO_4^{3-} mainly through three key reactions: 43,93,94 (a) the coprecipitation of Ca-U-P phases (e.g., autunite $[Ca(UO_2)_2(PO_4)_2\cdot 11H_2O)]$) at relatively higher uranyl concentrations $(10-100~\mu\text{M})$; (b) surface adsorption between sediment/precipitate and uranyl phosphates; and (c) incorpo-

ration into Ca–P precipitates when uranyl concentrations are low (\sim 1 μ M). ⁴⁴ In our studies, most of the 0.05 mM U was rapidly removed when stock solutions were mixed with Ca²⁺ and PO₄³⁻ supplements at both acid and neutral conditions. However, the competing effect of PO₄³⁻ enhanced the mobility of soluble As species, which has been explained by the chemical similarity between PO₄³⁻ and AsO₄³⁻ as oxyanious ^{49,95-97}

Aqueous Uranyl and Arsenate Removal with Ca-P Bearing Precipitates and Limestone at pH from 7.0 to 11.0. The concentrations of Ca (10 mM Ca²⁺) and P (2 mM PO₄³⁻) used here were higher than those used in the experiments presented in the previous subsection to promote HAp precipitation with an increasing pH from 7.0 to 11.0. Therefore, an abundance of white Ca-P precipitates was observed upon increasing pH. HAp precipitation was expected along with other Ca-P phases such as amorphous calcium phosphate and octacalcium phosphate from saturated solutions above pH 7.0.98 The initial pH of the system was between 5.0 and 7.0; NH₄OH was added to gradually increase the pH to the target range 7.0 to 11.0. At the beginning of the experiments (with an initial pH between 5 and 7, Figure S5), the concentration of uranyl decreased from 11,901 to 1.6 $\mu g/L$ in solutions without limestone (Figure 2C). In solutions with limestone, the uranyl concentration was decreased to 6.2 μ g/L (Figure 2 G). The minimum U concentrations measured in these experiments are below the EPA MCL of 30 ppb. Less than 3% of U was redissolved into the liquid phase at pH values higher than 9.0. More than 99% of aqueous As was removed in all solutions at the end point of pH 11.0. The lowest average concentration of As was measured to be 18 and 10.5 μ g/L in solutions with and without limestone, respectively, which is close to the EPA MCL of 10 ppb (Figure 2D,H). Under mild alkaline conditions (pH 9.0), arsenate removal ranged from 30 to 98%. The average removal was 55% for solutions with limestone and 95% for solutions without limestone. The presence of limestone resulted in a slight increase in Ca²⁺ concentration in solutions (Figure 2E), and the observed negative surface charge of limestone had a limited impact on the removal of aqueous U and As in this

The removal of uranyl was primarily attributed to the coprecipitation with ${\rm Ca}^{2+}$ and ${\rm PO_4}^{3-}$ ions, 43 while the removal of arsenate was facilitated by the precipitation of HAp. 63,64,99 The adsorption of As by HAp is potentially enhanced at high pH levels until it reaches around pH 8.0, which is close to the point of zero charge. However, the adverse effect of ${\rm PO_4}^{3-}$ addition on the removal of aqueous arsenate 64 was not observed in our study, as dissolved Ca promoted saturation with respect to Ca–P precipitates.

In the experiments of this subsection (pH ranging from 7.0 to 11.0), we observed a slight decrease in the solution's pH (less than 0.7 pH units) after 1 h of shaking, regardless of the presence of limestone (Supporting Information, Figure S6). The smallest average decrease in pH (less than 0.1 unit) was observed at pH values of 8.0 and 9.0. Aqueous Ca^{2+} and PO_4^{3-} decreased due to precipitation reactions when the pH rose from 7.0 to 8.0, and P concentrations were as low as the detection limit for ICP-OES at pH 9.0 (Figure 2A,B,E,F). The buffer effect of H_2PO4^{3-}/HPO_4^{2-} (p $K_{a2} = 7.21$) and $H_2AsO4^{3-}/HAsO_4^{2-}$ (p $K_{a2} = 6.69$) may have impacted the solution's pH between 7.0 and 8.0. However, under more alkaline conditions, the equilibrium of the solution with

atmospheric CO_2 could influence the decrease in pH. Another possibility is that the precipitation of HAp precursors and further transformation to HAp could affect solid hydration (incorporation of water into the solid structure), leading to the release or incorporation of H^+ and OH^- in solutions. Further research is required to elucidate the mechanisms affecting pH changes in this system.

Analyses for Solid Samples. Albite ((Na,Ca)(Si,Al)₄O₈), calcite (CaCO₃), quartz (SiO₂), and dolomite [MgCa(CO₃)₂] were identified by pXRD analyses for limestone solids collected before and after experiments presented in the previous subsections (Figure 3, separated diffractograms in

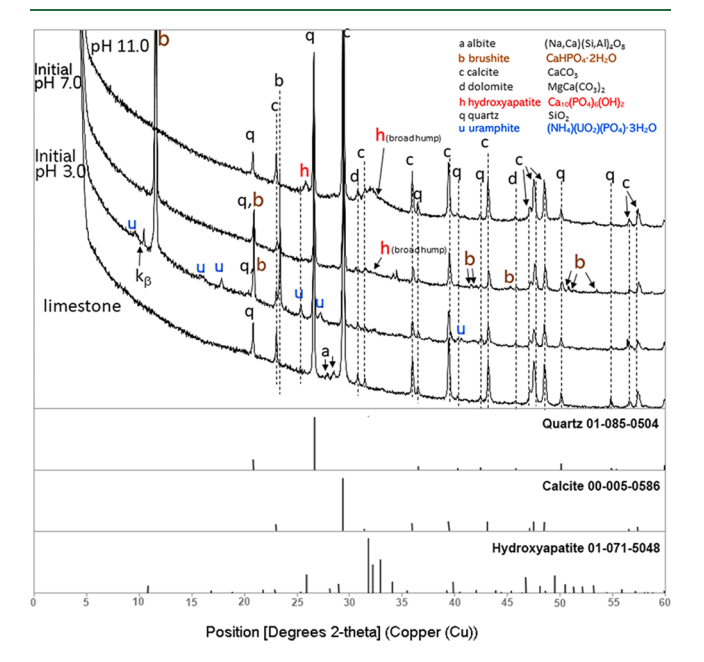


Figure 3. Diffractograms from powder X-ray diffraction (pXRD) are compared for solids collected from different conditions: 0.05 mM of U and As, 1 mM of PO_4^{3-} and 3 mM of Ca^{2+} with 1 g L^{-1} of limestone at initial pH 3.0 and 7.0; 0.05 mM of U and As, 2 mM of PO_4^{3-} , and 10 mM of Ca^{2+} with 1 g L^{-1} of limestone at pH 11.0. The limestone diffractogram is measured from grinded natural samples. Standard patterns of quartz, calcite, and hydroxyapatite are provided at bottom for reference.

Figures S7-S9). Two Ca-P minerals were identified as HAp [Ca₁₀(PO₄)₆(OH)₂] in precipitates at pH 11.0 and brushite [CaHPO₄·2H₂O] in samples of initial pH values of 3.0 and 7.0. Brushite has been reported as a precursor of HAp in another study, 100 and the transformation was observed under alkaline conditions. Since the precipitated HAp has poor crystallinity, HAp is indicated by a broad peak between 31 and 34° 2θ in the diffractogram for solids collected at pH 11. Analyses of pXRD data indicate that HAp is the dominant Ca-P phase at pH 11.0 with 10 mM Ca²⁺ and 2 mM PO₄³⁻. The peaks in the pXRD pattern corresponding to HAp are near the detection limit for samples with an initial pH of 7.0 with 3 mM Ca²⁺ and 1 mM PO₄³⁻. Instead, brushite is a minor contributor in the diffractogram. The uranyl phosphate, uramphite $(NH_4)(UO_2)$ -(PO₄)·3H₂O₄ was identified in solids collected from an initial pH of 3.0.

Various solid morphologies were observed using SEM where Ca and P were located, indicating the heterogeneous crystallinity of the calcium phosphate solid phases. Agglomerated nano- to microparticles in this study are consistent with

SEM images of HAp from previous studies. 62,101 The built-in backscattered electron detector (BSD) differentiates elements with brightness gradients based on their elemental weight, which also correlates with their atomic number. Brighter surfaces of Ca-P precipitates (Figure 4B) detected by SEM with BSD may indicate a higher concentration of U or As adsorbed onto the Ca-P solids than on the limestone. This observation supports the high affinity of HAp to aqueous uranyl and/or arsenate species reported in previous studies. 102 Analysis of EDX spectra detected the elements P, Ca, O, and Si that can be attributed to the precipitation of Ca-P, quartz, and calcite, along with other trace metals in limestone (Figure 4). Phosphorus EDX mappings were useful to distinguish Ca-P coatings (Figure 4A) and Ca-P particles (Figure 4B) from limestone. Low concentrations (less than 3 wt %) of U and As were observed on solid surfaces of limestone and Ca-P precipitates collected at pH 11.0 (Figure 4), as well as other samples collected with initial pH 3.0 and 7.0 (Supporting Information, Figures S10 and S11). A similar elemental distribution pattern was revealed by EDX maps between U and P, indicating their potential coprecipitation on the mineral surfaces. However, coexisting Al and K can interfere with the EDX quantification of U and As at low concentrations. 16,103 Thus, we also used EMA analyses as a complementary approach with a higher resolution to detect lower concentrations of U and As.

Elemental distributions of Ca, P, Cl, As, and U in HAp were further investigated by EMA analyses on a cross-section of a HAp-coated limestone grain from samples with 10 mM Ca²⁺ and 2 mM PO₄³⁻ at pH 11.0 (Figure 5). The HAp coating in mappings is observed with lower Ca and Cl concentrations but greater P compared to limestone. A consistent trend between elemental distributions of P and U is observed in crosssectional mappings, which is similar to the EDX observation on surfaces of Ca-P precipitates described in this section. Moreover, more co-occurrence of P and U was observed in samples of initial pH 3.0 and 7.0 with 3 mM Ca²⁺ and 1 mM PO₄³⁻ (Supporting Information, Figures S12 and S13). The uranium mapping indicates elevated U concentrations in the areas of the HAp coatings near the limestone-HAp interface. This suggests that U coprecipitated with P (and/or Ca) occurred during the initial stages of Ca-P precipitation, which agrees with the removal of U, Ca, and P detected by ICP-OES/ MS (Figure 2). In contrast, evenly distributed As is shown in the mapping of the cross-section, indicating a different removal mechanism compared to U.

Mechanisms of Uranyl and Arsenate Removal with Limestone, HAp, and Chemical Supplements. Different mechanisms influence the removal of aqueous uranyl and arsenate through reactions with limestone, HAp, PO₄³⁻, and Ca²⁺, depending on the concentration and pH conditions tested. For solutions with initial 1 mM U and As at pH 3.0, a portion of the U and As are removed by coprecipitation (Figure 1A). Uranyl arsenate minerals such as trögerite [(UO₂)(H₂AsO₄)₂(H₂O)] are expected under acidic conditions. 104,105 The presence of limestone neutralized acid solutions with an initial pH of 3.0 to approximately 7 at the end point and released soluble Ca2+ simultaneously. The addition of soluble Ca²⁺ ions provided by the acidic dissolution of calcite in limestone improved uranyl and arsenate removal by forming uranospinite [Ca(UO₂)₂(AsO₄)₂·10H₂O] precipitates that have been found to be relatively stable at acidic conditions in a previous study. 18 Water chemistry modeling

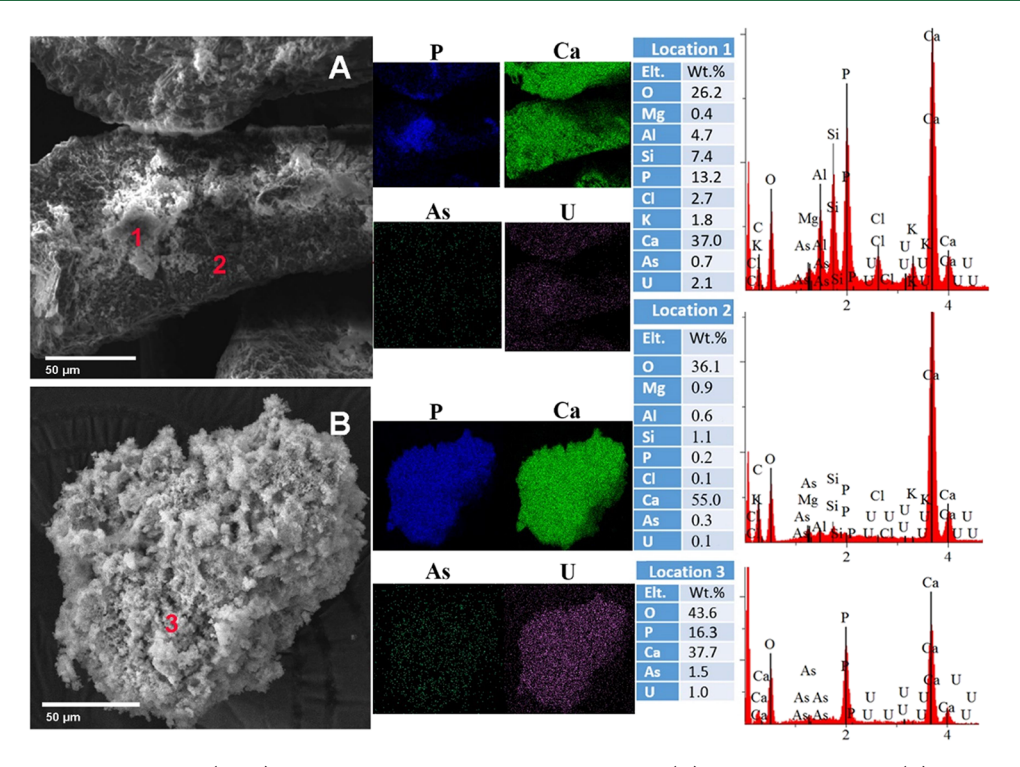


Figure 4. Scanning electron microscopy (SEM) images show the HAp-coated calcite grain (A) and a Ca-P particle (B) collected from 0.05 mM of U and As, 2 mM of PO₄³⁻, and 10 mM of Ca²⁺ with 1 g L⁻¹ of limestone at pH 11.0. Backscattered electron detector (BSD) was applied with energy dispersive X-ray (EDX) spectroscopy elemental mappings of P, Ca, As, and U, as well as spectra at selected locations.

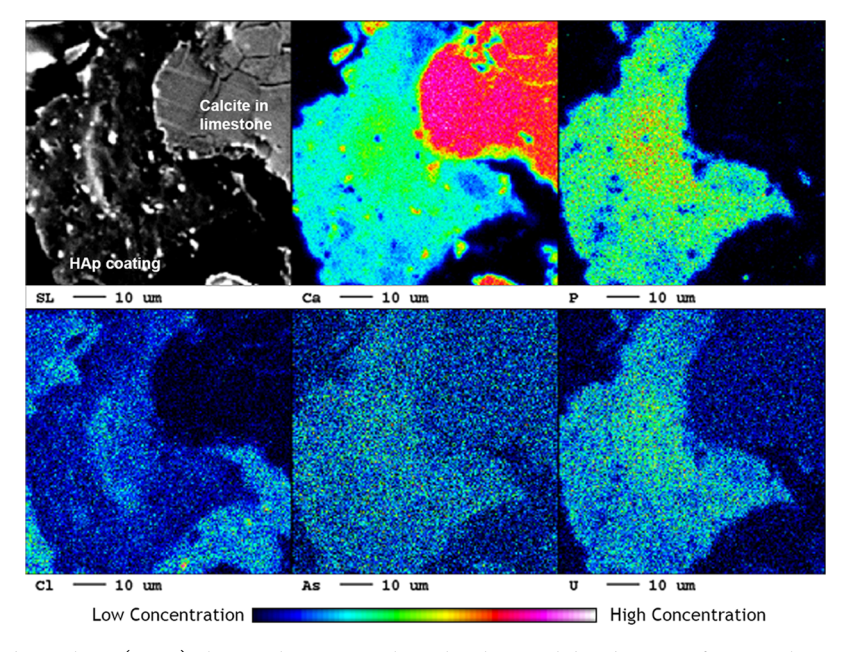


Figure 5. Electron microprobe analyzer (EMA) elemental mappings show the elemental distributions of Ca, P, Cl, As, and U at a cross-section of a HAp-coated calcite grain collected from 0.05 mM of U and As, 2 mM of PO_4^{3-} , and 10 mM of Ca^{2+} with 1 g L^{-1} of limestone at pH 11.0.

also indicates the possible precipitation of $Na_{0.5}(H_3O)_{0.5}[(UO_2)(AsO_4)](H_2O)_{2.5(s)}$ when sodium arsenate was applied as reported in another study.⁹²

Limestone has a greater influence on the removal of uranyl and arsenate in acidic environments than under circumneutral conditions (Figure 1A). In solutions with an initial pH of 3.0, limestone helped improve the removal from 80 to 96% for aqueous uranyl and from 60 to 100% for arsenate mainly through forming Ca–U–As precipitates with lesser contribu-

tion from surface adsorption. However, limestone is not an effective enhancer for the uranyl and arsenate removal in solutions with initial pH of 7.0 (Figure 1B) because fewer Ca ions are released into the solution by calcite dissolution and bicarbonate diffused from $\mathrm{CO}_{2(\mathrm{g})}$ may primarily complex with U to form highly soluble U–Ca–CO $_3$ aqueous complexes. ¹⁸

When 3 mM Ca^{2+} and 1 mM PO_4^{3-} are added, dominant uranyl coprecipitates become U-P solids such as chernikovite $[H_3O(UO_2)(PO_4)\cdot 3H_2O]$, ¹⁰⁶ autunite $[Ca(UO_2)_2(PO_4)_2\cdot$

 $11H_2O$], and uramphite [(NH₄)UO₂PO₄·3H₂O] in acidic conditions. $^{107-109}$ In our study, signals from uramphite are identified in the pXRD analysis for solid samples with an initial pH 3.0 (Figure 3). Given the high consistency between U and P elemental mappings in both EDX and EMA analyses (Figures 4 and 5), the rapid coprecipitation of uranyl phosphate is the main mechanism for uranyl removal. As a counteranion of AsO_4^{3-} , PO_4^{3-} inhibits As from coprecipitation with U and Ca. Based on the pXRD results (Figure 3), the concentrations of 3 mM Ca^{2+} and 1 mM PO_4^{3-} with initial pH 3.0 and 7.0 were not enough to achieve supersaturation with respect to HAp and, therefore, resulted in the limited removal of As (Figure 2C,D).

The addition of higher concentrations of Ca²⁺ (10 mM) and PO₄³⁻ (2 mM) reached supersaturation with respect to HAp at pH values ranging from 7.0 to 11.0. The gradual removal of aqueous arsenate in solutions (Figure 2F,H) was observed after white Ca-P precipitates started to form. Compared with the rapid removal of uranyl from solutions (Figure 2C,G), the removal of arsenate was mainly achieved by the adsorption of arsenate species to HAp. Moreover, the mechanism of ion exchange between AsO₄³⁻ anions and lattice PO₄³⁻ in HAp has been reported by related studies. 64,110 Evidence for the removal pathways of aqueous arsenate and uranyl can be found with EMA analyses in elemental distributions (Figure 5). A high consistency between Ca, P, and U in the crosssection of the HAp coating indicates possible coprecipitation. However, arsenic is scattered in the coating indicating a constant removal during the development of the HAp coating. Most of the PO₄³⁻ was precipitated with Ca²⁺ at pH values rising from 7 to 9 to form HAp as well as other Ca-P precipitation that removed between 62.7 and 98.4% aqueous arsenate at pH 9.

Although effective removal of aqueous uranyl and arsenate was achieved at pH 9.0 through reactions with limestone and HAp, slight dissolution of uranyl was observed as the solution pH increased beyond 9.0 (Figure 2C,G). Given that redissolved U (less than 600 μ g L⁻¹) was much lower than its total concentration of 0.05 mM uranyl (11,901 μ g L⁻¹), carbonate can enhance the mobilization of uranyl by complexing the surface fraction associated with HAp or limestone, which increased lability at pH higher than 8.111 Additionally, the adsorption of arsenate to HAp can be limited by the negative net surface charge at pH higher than 8.63 To increase the reactivity of HAp and limestone for the immobilization of uranyl and arsenate mixtures through identified mechanisms, it is important to maintain a solution pH between 8 and 9 and supersaturated Ca²⁺ and PO₄³⁻ concentrations for HAp precipitation.

Environmental Implications. This study presents a method for removing aqueous uranyl arsenate mixtures by reacting them with natural limestone supplemented with Ca²⁺ and PO₄³⁻ to promote supersaturation with respect to HAp at optimal pH ranging from 8.0 to 9.0. Aqueous uranyl was predominantly removed through coprecipitation with additional Ca²⁺ and PO₄³⁻ in solutions, while arsenate was immobilized through adsorption reactions with precipitated HAp. This approach shows promise for treating sites affected by a mining legacy. For example, co-occurrence of uranyl and arsenate at pH ranging from 6.8 to 8.6 has been found in sites located in tribal land in New Mexico and Arizona.^{2,16,34} The widespread occurrence of limestone in mine sites is advantageous for the reactions evaluated in this study. The reaction of

uranyl and arsenate with naturally occurring materials, such as limestone and HAp could be considered as a potential remediation strategy. Future studies should investigate the performance of naturally occurring minerals under flow conditions and environmentally relevant conditions for the development of remediation methods that can be accessible to under-served communities.

ASSOCIATED CONTENT

Supporting Information

The Supporting Information is available free of charge at https://pubs.acs.org/doi/10.1021/acs.est.3c03809.

Additional text providing more detailed experimental methods for ICP-OES/MS, acid digestion, BET analysis, pXRD, SEM-EDX, and EMA; detailed information on chemicals used in this study; results for additional analyses for natural limestone including average elemental compositions measured by EMA; chemical equilibrium modeling results for predominant soluble species of U and As; mineralogy analyses by pXRD; zeta potential; detailed pH data as a function a time; modeling results for saturation indices of U and As solids; detailed pXRD raw data and interpretation for potential solid phases; and supplemental elemental data for surface elements detected by EDX and EMA (PDF)

AUTHOR INFORMATION

Corresponding Authors

Han Hua – Department of Civil, Construction & Environmental Engineering and Center for Water and the Environment, University of New Mexico, Albuquerque, New Mexico 87131, United States; ◎ orcid.org/0000-0002-0567-4210; Email: hh99@unm.edu

José M. Cerrato — Department of Civil, Construction & Environmental Engineering and Center for Water and the Environment, University of New Mexico, Albuquerque, New Mexico 87131, United States; UNM Metals Exposure and Toxicity Assessment on Tribal Lands in the Southwest (UNM METALS) Superfund Research Program Center, Albuquerque, New Mexico 87131, United States; orcid.org/0000-0002-2473-6376; Email: jcerrato@unm.edu

Authors

Isabel Meza – Department of Civil, Construction & Environmental Engineering and Center for Water and the Environment, University of New Mexico, Albuquerque, New Mexico 87131, United States

Kaelin Gagnon – Department of Civil, Construction & Environmental Engineering and Center for Water and the Environment, University of New Mexico, Albuquerque, New Mexico 87131, United States

Anjali Mulchandani — Department of Civil, Construction & Environmental Engineering and Center for Water and the Environment, University of New Mexico, Albuquerque, New Mexico 87131, United States; Occid.org/0000-0001-6529.8336

Jorge Gonzalez-Estrella — School of Civil and Environmental Engineering, College of Engineering, Architecture, and Technology, Oklahoma State University, Stillwater, Oklahoma 74078, United States; orcid.org/0000-0002-4873-0454

- Peter C. Burns Department of Civil and Environmental Engineering and Earth Sciences and Department of Chemistry and Biochemistry, University of Notre Dame, Notre Dame, Indiana 46556, United States; orcid.org/0000-0002-2319-9628
- Abdul-Mehdi S. Ali Department of Earth and Planetary Sciences, MSC03 2040, University of New Mexico, Albuquerque, New Mexico 87131, United States
- Michael Spilde Department of Earth and Planetary Sciences, MSC03 2040, University of New Mexico, Albuquerque, New Mexico 87131, United States
- Eric Peterson Department of Earth and Planetary Sciences, MSC03 2040, University of New Mexico, Albuquerque, New Mexico 87131, United States
- Peter Lichtner Center for Water and the Environment, University of New Mexico, Albuquerque, New Mexico 87131, United States

Complete contact information is available at: https://pubs.acs.org/10.1021/acs.est.3c03809

Notes

The authors declare no competing financial interest.

ACKNOWLEDGMENTS

The funding for this research was provided by the National Science Foundation (CAREER Award 1652619, CREST Award 1914490) the University of New Mexico Comprehensive Cancer Center and College of Pharmacy, and by the National Institute of Environmental Health Sciences of the National Institutes of Health under the Superfund Research Program Award Number P42ES025589. The contribution of P.C.B. to this work was funded by the Chemical Sciences, Geosciences and Biosciences Division, Office of Basic Energy Sciences, Office of Science, U.S. Department of Energy, Grant No. DE-FG02-07ER15880. Partial fudging for the PerkinElmer NexION ICP/MS coupled with the ESI SeaFast SP3 was provided by the UNM Office of the Vice President for Research (OVPR) and the College of Art and Sciences. We also would like to acknowledge PerkinElmer and ESI for their valuable technical and application support for the use of their analytical instruments to support this research project and provide quality data. Electron microprobe and scanning transmission electron microscopy were performed in the Electron Microbeam Analysis Facility, Department of Earth and Planetary Sciences and Institute of Meteoritics, University of New Mexico, a facility supported by the State of New Mexico, National Aeronautics and Space Administration (NASA), and the National Science Foundation. Any opinions, findings, and conclusions or recommendations expressed in this publication are those of the author(s) and do not necessarily reflect the views of the National Science Foundation, the National Institutes of Health, or the U.S. Department of Energy.

REFERENCES

- (1) Dzik, E. A.; Lobeck, H. L.; Zhang, L.; Burns, P. C. Thermodynamic properties of phosphate members of the meta-autunite group: A high-temperature calorimetric study. *J. Chem. Thermodyn.* **2017**, *114*, 165–171.
- (2) Blake, J. M.; Avasarala, S.; Ali, A.-M. S.; Spilde, M.; Lezama-Pacheco, J. S.; Latta, D.; Artyushkova, K.; Ilgen, A. G.; Shuey, C.; Nez, C.; Cerrato, J. M. Reactivity of As and U co-occurring in mine wastes in northeastern Arizona. *Chem. Geol.* **2019**, *522*, 26–37.

- (3) Corkhill, C. L.; Crean, D. E.; Bailey, D. J.; Makepeace, C.; Stennett, M. C.; Tappero, R.; Grolimund, D.; Hyatt, N. C. Multi-scale investigation of uranium attenuation by arsenic at an abandoned uranium mine, South Terras. *npj Mater. Degrad.* **2017**, *1* (1), 19.
- (4) Martinez-Morata, I.; Bostick, B. C.; Conroy-Ben, O.; Duncan, D. T.; Jones, M. R.; Spaur, M.; Patterson, K. P.; Prins, S. J.; Navas-Acien, A.; Nigra, A. E. Nationwide geospatial analysis of county racial and ethnic composition and public drinking water arsenic and uranium. *Nat. Commun.* **2022**, *13* (1), 7461.
- (5) Crowley, K. D. Managing the Environmental Legacy of US Nuclear-Weapons Production: Although the waste from America's arms buildup will never be" cleaned up," human and environmental risks can be reduced and managed. *Am. Sci.* **2002**, *90* (6), 514.
- (6) USEPA, Federal Actions to Address Impacts of Uranium Contamination in the Navajo Nation Five-Year Plan Summary Report. In US Environmental Protection Agency: Pacific Southwest, Region 9: San Francisco CA. 2013.
- (7) NRC Uranium mining in Virginia: scientific, technical, environmental, human health and safety, and regulatory aspects of uranium mining and processing in Virginia; National Research Council. National Academies Press: 2012.
- (8) Hund, L.; Bedrick, E. J.; Miller, C.; Huerta, G.; Nez, T.; Ramone, S.; Shuey, C.; Cajero, M.; Lewis, J. A Bayesian framework for estimating disease risk due to exposure to uranium mine and mill waste on the Navajo Nation. *J. R. Stat. Soc. Ser. A-Stat. Soc.* **2015**, *178* (4), 1069–1091.
- (9) Schmoker, J. W.; Krystinik, K. B.; Halley, R. B. Selected characteristics of limestone and dolomite reservoirs in the United-States. *AAPG Bull.* **1985**, *69* (5), 733–741.
- (10) Allan, R. J., Impact of Mining Activities on the Terrestrial and Aquatic Environment with Emphasis on Mitigation and Remedial Measures. In *Heavy Metals: Problems and Solutions*, Förstner, U.; Salomons, W.; Mader, P., Eds.; Springer Berlin Heidelberg: Berlin, Heidelberg, 1995; 119–140.
- (11) Wufuer, R.; Wei, Y.; Lin, Q.; Wang, H.; Song, W.; Liu, W.; Zhang, D.; Pan, X.; Gadd, G. M., Chapter Four Uranium Bioreduction and Biomineralization. In *Adv. Appl. Microbiol*, Sariaslani, S.; Gadd, G. M., Eds.; Academic Press: 2017; *101*, 137–168.
- (12) Kapaj, S.; Peterson, H.; Liber, K.; Bhattacharya, P. Human Health Effects From Chronic Arsenic Poisoning—A Review. *J. Environ. Sci. Part A* **2006**, *41* (10), 2399—2428.
- (13) Agency, E. P., National Primary Drinking Water Regulations. In *Regulations*, N, P. D. W., Ed.; Environmental Protection Agency, 2019.
- (14) USEPA, Addressing uranium contamination on the Navajo Nation. U.S. In Environmental Protection Agency, Pacific Southwest, Region 9.: San Francisco, CA, 2015.
- (15) Avasarala, S.; Lichtner, P. C.; Ali, A.-M. S.; González-Pinzón, R.; Blake, J. M.; Cerrato, J. M. Reactive Transport of U and V from Abandoned Uranium Mine Wastes. *Environ. Sci. Technol.* **2017**, *51* (21), 12385–12393.
- (16) Blake, J. M.; Avasarala, S.; Artyushkova, K.; Ali, A.-M. S.; Brearley, A. J.; Shuey, C.; Robinson, W. P.; Nez, C.; Bill, S.; Lewis, J. Elevated concentrations of U and co-occurring metals in abandoned mine wastes in a northeastern Arizona Native American community. *Environ. Sci. Technol.* **2015**, *49* (14), 8506–8514.
- (17) DeVore, C.; Freire, L. R.; Gonzalez-Estrella, J.; Villa, N.; Ali, A. M.; Ducheneaux, C.; Artyushkova, K.; Cerrato, J. Investigation of the effect of microbial processes on arsenic stability in sediments from Cheyenne River, South Dakota, USA. *Abstr. Pap. Am. Chem. Soc.* **2019**, 257, 1.
- (18) Gonzalez-Estrella, J.; Meza, I.; Burns, A. J.; Ali, A.-M. S.; Lezama-Pacheco, J. S.; Lichtner, P.; Shaikh, N.; Fendorf, S.; Cerrato, J. M. Effect of bicarbonate, calcium, and pH on the reactivity of As(V) and U(VI) mixtures. *Environ. Sci. Technol.* **2020**, *54*, 3979.
- (19) Dixit, S.; Hering, J. G. Comparison of arsenic (V) and arsenic (III) sorption onto iron oxide minerals: implications for arsenic mobility. *Environ. Sci. Technol.* **2003**, 37 (18), 4182–4189.

- (20) Troyer, L. D.; Stone, J. J.; Borch, T. Effect of biogeochemical redox processes on the fate and transport of As and U at an abandoned uranium mine site: an X-ray absorption spectroscopy study. *Environ. Chem.* **2014**, *11* (1), 18–27.
- (21) Gimenez, J.; Martínez, M.; de Pablo, J.; Rovira, M.; Duro, L. Arsenic sorption onto natural hematite, magnetite, and goethite. *J. Hazard. Mater.* **2007**, 141 (3), 575–580.
- (22) Velasco, C. A.; Brearley, A. J.; Gonzalez-Estrella, J.; Ali, A.-M. S.; Meza, M. I.; Cabaniss, S. E.; Thomson, B. M.; Forbes, T. Z.; Lezama Pacheco, J. S.; Cerrato, J. M. From adsorption to precipitation of U (VI): what is the role of pH and natural organic matter? *Environ. Sci. Technol.* **2021**, *55* (23), 16246–16256.
- (23) Jerden, J. L., Jr; Sinha, A. Geochemical coupling of uranium and phosphorous in soils overlying an unmined uranium deposit: Coles Hill, Virginia. *J. Geochem. Explor.* **2006**, *91* (1–3), 56–70.
- (24) Davis, J.; Payne, T.; Waite, T. Geochemisty of soil radionuclides. Soil Sci. Soc. Am., Madison, WI 2015, 61–86.
- (25) Barnett, M.; Jardine, P.; Brooks, S.; Selim, H. Adsorption and transport of uranium (VI) in subsurface media. *Soil Sci. Soc. Am. J.* **2000**, *64* (3), 908–917.
- (26) Barnett, M. O.; Jardine, P. M.; Brooks, S. C. U (VI) adsorption to heterogeneous subsurface media: application of a surface complexation model. *Environ. Sci. Technol.* **2002**, *36* (5), 937–942.
- (27) Nazari, A. M.; Radzinski, R.; Ghahreman, A. Review of arsenic metallurgy: Treatment of arsenical minerals and the immobilization of arsenic. *Hydrometallurgy* **2017**, *174*, 258–281.
- (28) Fendorf, S.; Nico, P. S.; Kocar, B. D.; Masue, Y.; Tufano, K. J. Arsenic chemistry in soils and sediments. *Dev. Soil Sci.* **2010**, *34*, 357–378, DOI: 10.1016/S0166-2481(10)34012-8.
- (29) Selvakumar, R.; Ramadoss, G.; Menon, M. P.; Rajendran, K.; Thavamani, P.; Naidu, R.; Megharaj, M. Challenges and complexities in remediation of uranium contaminated soils: A review. *J. Environ. Radioactiv.* **2018**, *192*, 592–603.
- (30) Satpathy, A.; Catalano, J. G.; Giammar, D. E. Reduction of U (VI) on chemically reduced montmorillonite and surface complexation modeling of adsorbed U (IV). *Environ. Sci. Technol.* **2022**, *56* (7), 4111–4120.
- (31) Wu, Q.; Jiang, X.; Wu, H.; Zou, L.; Wang, L.; Shi, J. Effects and Mechanisms of Copper Oxide Nanoparticles with Regard to Arsenic Availability in Soil–Rice Systems: Adsorption Behavior and Microbial Response. *Environ. Sci. Technol.* **2022**, *56* (12), 8142–8154.
- (32) Frost, R. L.; Carmody, O.; Erickson, K. L.; Weier, M. L. Near-infrared spectroscopy to uranyl arsenates of the autunite and metaautunite group. *Spectrochimica Acta Part A: Molecular and Biomolecular Spectroscopy* **2005**, *61* (8), 1923–1927.
- (33) Bachmaf, S.; Merkel, B. J. Sorption of uranium (VI) at the clay mineral—water interface. *Environ. Earth Sci.* **2011**, *6*3 (5), 925–934.
- (34) Blake, J. M.; De Vore, C. L.; Avasarala, S.; Ali, A.-M.; Roldan, C.; Bowers, F.; Spilde, M. N.; Artyushkova, K.; Kirk, M. F.; Peterson, E. Uranium mobility and accumulation along the Rio Paguate, Jackpile mine in Laguna Pueblo, NM. *Environ. Sci. Processes Impacts* 2017, 19 (4), 605–621.
- (35) Dong, W.; Brooks, S. C. Determination of the formation constants of ternary complexes of uranyl and carbonate with alkaline earth metals (Mg²⁺, Ca²⁺, Sr²⁺, and Ba²⁺) using anion exchange method. *Environ. Sci. Technol.* **2006**, *40* (15), 4689–4695.
- (36) Ulrich, K.-U.; Ilton, E. S.; Veeramani, H.; Sharp, J. O.; Bernier-Latmani, R.; Schofield, E. J.; Bargar, J. R.; Giammar, D. E. Comparative dissolution kinetics of biogenic and chemogenic uraninite under oxidizing conditions in the presence of carbonate. *Geochim. Cosmochim. Ac.* 2009, 73 (20), 6065–6083.
- (37) Meza, I.; Jemison, N.; Gonzalez-Estrella, J.; Burns, P. C.; Rodriguez, V.; Sigmon, G. E.; Szymanowski, J. E.; Ali, A.-M. S.; Gagnon, K.; Cerrato, J. M. Kinetics of Na-and K-uranyl arsenate dissolution. *Chem. Geol.* **2023**, *636*, No. 121642.
- (38) Castor, S. B.; Henry, C. D. Geology, geochemistry, and origin of volcanic rock-hosted uranium deposits in northwestern Nevada and southeastern Oregon, USA. *Ore Geol. Rev.* **2000**, *16* (1–2), 1–40.

- (39) Roshani, M.; Mirjalili, K. Studies on the leaching of an arsenic—uranium ore. *Hydrometallurgy* **2009**, *98* (3–4), 304–307.
- (40) Kaya, A.; Yukselen, Y. Zeta potential of clay minerals and quartz contaminated by heavy metals. *Can. Geotech. J.* **2005**, 42 (5), 1280–1289
- (41) Jie, Z.; Weiqing, W.; Jing, L.; Yang, H.; Qiming, F.; Hong, Z. Fe (III) as an activator for the flotation of spodumene, albite, and quartz minerals. *Miner. Eng.* **2014**, *61*, 16–22.
- (42) Alroudhan, A.; Vinogradov, J.; Jackson, M. D. Zeta potential of intact natural limestone: Impact of potential-determining ions Ca, Mg and SO4. *Colloids Surf. A: Physicochem. Eng. Asp.* **2016**, 493, 83–98.
- (43) Mehta, V. S.; Maillot, F.; Wang, Z.; Catalano, J. G.; Giammar, D. E. Effect of reaction pathway on the extent and mechanism of uranium (VI) immobilization with calcium and phosphate. *Environ. Sci. Technol.* **2016**, *50* (6), 3128–3136.
- (44) Wen, H.; Pan, Z.; Giammar, D.; Li, L. Enhanced uranium immobilization by phosphate amendment under variable geochemical and flow conditions: Insights from reactive transport modeling. *Environ. Sci. Technol.* **2018**, *52* (10), 5841–5850.
- (45) Pan, Z.; Giammar, D. E.; Mehta, V.; Troyer, L. D.; Catalano, J. G.; Wang, Z. Phosphate-induced immobilization of uranium in Hanford sediments. *Environ. Sci. Technol.* **2016**, *50* (24), 13486–13494.
- (46) Bai, Y.; Yang, T.; Liang, J.; Qu, J. The role of biogenic Fe-Mn oxides formed in situ for arsenic oxidation and adsorption in aquatic ecosystems. *Water Res.* **2016**, *98*, 119–127.
- (47) Mohamed, C.; Mohamed, Z.; Gabriela, C.; Fouad, S. Application of low-cost adsorbents for arsenic removal: A review. *J. Environ. Chem. Ecotoxicol.* **2012**, *4* (5), 91–102.
- (48) Sosa, A.; Armienta, M. A.; Aguayo, A.; Cruz, O. Evaluation of the influence of main groundwater ions on arsenic removal by limestones through column experiments. *Sci. Total Environ.* **2020**, 727, No. 138459.
- (49) DeVore, C. L.; Rodriguez-Freire, L.; Mehdi-Ali, A.; Ducheneaux, C.; Artyushkova, K.; Zhou, Z.; Latta, D. E.; Lueth, V. W.; Gonzales, M.; Lewis, J. Effect of bicarbonate and phosphate on arsenic release from mining-impacted sediments in the Cheyenne River watershed, South Dakota, USA. *Environ. Sci. Processes Impacts* 2019, 21 (3), 456–468.
- (50) MCLeMoRe, V. T.; HiLL, B.; KHaLSa, N.; Lucas Kamat, S. In Uranium resources in the Grants uranium district, New Mexico: An update, New Mexico Geological Society Guidebook. [64th Field Conference], Geology of Route, 2013; 2013.
- (51) Rawson, R. Uranium in Todilto Limestone (Jurassic) of New Mexico: example of a Sabkha-Like Deposit *Mem.-NM Bur. Mines Miner. Resour.*; (United States) 1980, 38 CONF-7905120-.
- (52) Bhalara, P. D.; Punetha, D.; Balasubramanian, K. A review of potential remediation techniques for uranium (VI) ion retrieval from contaminated aqueous environment. *J. Environ. Chem. Eng.* **2014**, 2 (3), 1621–1634.
- (53) Mohan, D.; Pittman, C. U., Jr Arsenic removal from water/wastewater using adsorbents—a critical review. J. Hazard. Mater. 2007. 142 (1-2), 1-53.
- (54) Sdiri, A.; Higashi, T.; Jamoussi, F.; Bouaziz, S. Effects of impurities on the removal of heavy metals by natural limestones in aqueous systems. *J. Environ. Manage.* **2012**, 93 (1), 245–253.
- (55) Sø, H. U.; Postma, D.; Jakobsen, R.; Larsen, F. Sorption and desorption of arsenate and arsenite on calcite. *Geochim. Cosmochim. Acta* **2008**, 72 (24), 5871–5884.
- (56) Alexandratos, V. G.; Elzinga, E. J.; Reeder, R. J. Arsenate uptake by calcite: macroscopic and spectroscopic characterization of adsorption and incorporation mechanisms. *Geochim. Cosmochim. Ac.* **2007**, *71* (17), 4172–4187.
- (57) Alroudhan, A.; Vinogradov, J.; Jackson, M. Zeta potential of intact natural limestone: Impact of potential-determining ions Ca, Mg and SO4. *Colloid. Surfaces A: Physicochemical and Engineering Aspects* **2016**, 493, 83–98.

- (58) Corami, A.; Mignardi, S.; Ferrini, V. Cadmium removal from single-and multi-metal (Cd+ Pb+ Zn+ Cu) solutions by sorption on hydroxyapatite. *J. Colloid Interface Sci.* **2008**, 317 (2), 402–408.
- (59) Piccoli, P. M.; Candela, P. A. Apatite in igneous systems. *Rev. Mineral. Geochem.* **2002**, 48 (1), 255–292.
- (60) Pu'ad, N. M.; Koshy, P.; Abdullah, H.; Idris, M.; Lee, T. Syntheses of hydroxyapatite from natural sources. *Heliyon* **2019**, *5* (5), No. e01588.
- (61) Shen, H.-Z.; Guo, N.; Zhao, L.; Shen, P. Role of ion substitution and lattice water in the densification of cold-sintered hydroxyapatite. *Scr. Mater.* **2020**, *177*, 141–145.
- (62) Sadat-Shojai, M.; Khorasani, M.-T.; Dinpanah-Khoshdargi, E.; Jamshidi, A. Synthesis methods for nanosized hydroxyapatite with diverse structures. *Acta biomater.* **2013**, *9* (8), 7591–7621.
- (63) Mirhosseini, M.; Biazar, E.; Saeb, K. Removal of arsenic from drinking water by hydroxyapatite nano particles. *Curr. World Environ.* **2014**, 9 (2), 331.
- (64) Islam, M.; Mishra, P. C.; Patel, R. Arsenate removal from aqueous solution by cellulose-carbonated hydroxyapatite nanocomposites. *J. Hazard. Mater.* **2011**, *189* (3), 755–763.
- (65) Su, M.; Tsang, D. C.; Ren, X.; Shi, Q.; Tang, J.; Zhang, H.; Kong, L.; Song, G.; Chen, D. Removal of U (VI) from nuclear mining effluent by porous hydroxyapatite: Evaluation on characteristics, mechanisms and performance. *Environ. Pollut.* **2019**, 254, 112891.
- (66) Fernando, M. S.; de Silva, R. M.; De Silva, K. N. Synthesis, characterization, and application of nano hydroxyapatite and nanocomposite of hydroxyapatite with granular activated carbon for the removal of Pb2+ from aqueous solutions. *Appl. Surf. Sci.* **2015**, *351*, 95–103.
- (67) Rout, S.; Muduli, B.; Kumar, A.; Pulhani, V. Removal of uranium (VI) from water using hydroxyapatite coated activated carbon powder nanocomposite. *J. Environ. Sci. Health, Part A* **2020**, 55 (5), 596–605.
- (68) Hokkanen, S.; Bhatnagar, A.; Srivastava, V.; Suorsa, V.; Sillanpää, M. Removal of Cd2+, Ni2+ and PO43– from aqueous solution by hydroxyapatite-bentonite clay-nanocellulose composite. *Int. J. Biol. Macromol.* **2018**, *118*, 903–912.
- (69) Zeng, H.; Lu, L.; Gong, Z.; Guo, Y.; Mo, J.; Zhang, W.; Li, H. Nanoscale composites of hydroxyapatite coated with zero valent iron: preparation, characterization and uranium removal. *J. Radioanal. Nucl. Chem.* **2019**, 320 (1), 165–177.
- (70) Yang, H.; Masse, S.; Zhang, H.; Hélary, C.; Li, L.; Coradin, T. Surface reactivity of hydroxyapatite nanocoatings deposited on iron oxide magnetic spheres toward toxic metals. *J. Colloid Interface Sci.* **2014**, *417*, 1–8.
- (71) Vila, M.; Sánchez-Salcedo, S.; Cicuéndez, M.; Izquierdo-Barba, I.; Vallet-Regí, M. Novel biopolymer-coated hydroxyapatite foams for removing heavy-metals from polluted water. *J. Hazard. Mater.* **2011**, 192 (1), 71–77.
- (72) Meski, S.; Ziani, S.; Khireddine, H. Removal of lead ions by hydroxyapatite prepared from the egg shell. *J. Chem. Eng. Data* **2010**, 55 (9), 3923–3928.
- (73) Liao, D.; Zheng, W.; Li, X.; Yang, Q.; Yue, X.; Guo, L.; Zeng, G. Removal of lead (II) from aqueous solutions using carbonate hydroxyapatite extracted from eggshell waste. *J. Hazard. Mater.* **2010**, 177 (1–3), 126–130.
- (74) Bee, S.-L.; Hamid, Z. A. Hydroxyapatite derived from food industry bio-wastes: Syntheses, properties and its potential multifunctional applications. *Ceram. Int.* **2020**, 46 (11), 17149–17175.
- (75) Brunauer, S. Adsorption of gases in multimolecular layers. J. Am. Chem. Soc. 1938, 60 (2), 309.
- (76) Nordstrom, D. K. Questa Baseline and Pre-mining Ground-water Quality Investigation 25. Summary of Results and Baseline and Pre-mining Ground-water Geochemistry, Red River Valley, Taos County, NM, 2001–2005, US Geological Survey: 2008.
- (77) Verplanck, P. L.; Nordstrom, D. K.; Bove, D. J.; Plumlee, G. S.; Runkel, R. L. Naturally acidic surface and ground waters draining porphyry-related mineralized areas of the Southern Rocky Mountains. *Colorado and New Mexico. Appl. Geochemistry* **2009**, 24 (2), 255–267.

- (78) Larson, L. N.; Kipp, G. G.; Mott, H. V.; Stone, J. J. Sediment pore-water interactions associated with arsenic and uranium transport from the North Cave Hills mining region, South Dakota, USA. *Appl. Geochem.* **2012**, 27 (4), 879–891.
- (79) Ruiz, O.; Thomson, B. M.; Cerrato, J. Investigation of In-Situ Leach (ISL) Mining of Uranium in New Mexico and Post-Mining Reclamation. *New Mexico Geol.* **2016**, *38* (4), 77–85.
- (80) Donahue, R.; Hendry, M. Geochemistry of arsenic in uranium mine mill tailings, Saskatchewan, Canada. *Appl. Geochem.* **2003**, *18* (11), 1733–1750.
- (81) Robertson, J.; Hendry, M. J.; Kotzer, T.; Hughes, K. A. Geochemistry of uranium mill tailings in the Athabasca Basin, Saskatchewan, Canada: A review. *Critical Reviews in Environ. Sci. Technol.* **2019**, 49 (14), 1237–1293.
- (82) Pfeifle, B. D.; Stamm, J. F.; Stone, J. J. Arsenic geochemistry of alluvial sediments and pore waters affected by mine tailings along the Belle Fourche and Cheyenne River floodplains. *Wat. Air Soil Pollut.* **2018**, 229, 183.
- (83) Lichtner, P.; Hammond, G.; Lu, C.; Karra, S.; Bisht, G.; Andre, B.; Mills, R.; Kumar, J.; Frederick, J., *PFLOTRAN User Manual. Technical Report.* 2019.
- (84) Gorman-Lewis, D.; Burns, P. C.; Fein, J. B. Review of uranyl mineral solubility measurements. *J. Chem. Thermodyn.* **2008**, 40 (3), 335–352.
- (85) Nipruk, O. V.; Chernorukov, N. G.; Elipasheva, E. V.; Klinshova, K. A.; Bakhmetev, M. O. State of uranyl arsenates M^1AsUO_6 nH_2O (M^1-H+ , Li+, Na+, K+, Rb+, Cs+, NH_4+) in aqueous solution. *J. Radioanal. Nucl. Chem.* **2020**, 324 (1), 233–244.
- (86) Dong, W.; Brooks, S. C. Formation of aqueous MgUO₂ (CO₃) ^{3⁻⁻} complex and uranium anion exchange mechanism onto an exchange resin. *Environ. Sci. Technol.* **2008**, 42 (6), 1979–1983.
- (87) Guillaumont, R.; Mompean, F. J. Update on the chemical thermodynamics of uranium, neptunium, plutonium, americium and technetium; Elsevier: Amsterdam, 2003; 5.
- (88) He, M.; Liu, X.; Cheng, J.; Lu, X.; Zhang, C.; Wang, R. Uranyl arsenate complexes in aqueous solution: Insights from first-principles molecular dynamics simulations. *Inorg. Chem.* **2018**, *57* (10), 5801–5809
- (89) Eriksson, R.; Merta, J.; Rosenholm, J. B. The calcite/water interface: I. Surface charge in indifferent electrolyte media and the influence of low-molecular-weight polyelectrolyte. *J. Colloid Interface Sci.* **2007**, 313 (1), 184–193.
- (90) Xu, N.; Yin, H.; Chen, Z.; Liu, S.; Chen, M.; Zhang, J. Mechanisms of phosphate retention by calcite: Effects of magnesium and pH. *J. Soils Sediments* **2014**, *14* (3), 495–503.
- (91) Pokrovsky, O.; Mielczarski, J.; Barres, O.; Schott, J. Surface speciation models of calcite and dolomite/aqueous solution interfaces and their spectroscopic evaluation. *Langmuir* **2000**, *16* (6), 2677–2688.
- (92) Meza, I.; Gonzalez-Estrella, J.; Burns, P. C.; Rodriguez, V.; Velasco, C. A.; Sigmon, G. E.; Szymanowski, J. E.; Forbes, T. Z.; Applegate, L. M.; Ali, A.-M. S. Solubility and Thermodynamic Investigation of Meta-Autunite Group Uranyl Arsenate Solids with Monovalent Cations Na and K. *Environ. Sci. Technol.* **2022**, *57*, 255–265, DOI: 10.1021/acs.est.2c06648.
- (93) Jerden, J., Jr; Sinha, A.; Zelazny, L. Natural immobilization of uranium by phosphate mineralization in an oxidizing saprolite—soil profile: chemical weathering of the Coles Hill uranium deposit, Virginia. *Chem. Geol.* **2003**, *199* (1–2), 129–157.
- (94) Ohnuki, T.; Kozai, N.; Samadfam, M.; Yasuda, R.; Yamamoto, S.; Narumi, K.; Naramoto, H.; Murakami, T. The formation of autunite (Ca (UO2) 2 (PO4) 2nH2O) within the leached layer of dissolving apatite: incorporation mechanism of uranium by apatite. *Chem. Geol.* 2004, 211 (1–2), 1–14.
- (95) Zeng, H.; Fisher, B.; Giammar, D. E. Individual and competitive adsorption of arsenate and phosphate to a high-surface-area iron oxide-based sorbent. *Environ. Sci. Technol.* **2008**, 42 (1), 147–152.

- (96) Aziz, Z.; Van Geen, A.; Stute, M.; Versteeg, R.; Horneman, A.; Zheng, Y.; Goodbred, S.; Steckler, M.; Weinman, B.; Gavrieli, I. Impact of local recharge on arsenic concentrations in shallow aquifers inferred from the electromagnetic conductivity of soils in Araihazar, Bangladesh. *Water Resour. Res.* **2008**, 44 (7), No. 006000, DOI: 10.1029/2007WR006000.
- (97) Das, N.; Patel, A. K.; Deka, G.; Das, A.; Sarma, K. P.; Kumar, M. Geochemical controls and future perspective of arsenic mobilization for sustainable groundwater management: a study from Northeast India. *Groundw. Sustain. Dev.* **2015**, *1* (1–2), 92–104.
- (98) Recillas, S.; Rodríguez-Lugo, V.; Montero, M.; Viquez-Cano, S.; Hernandez, L.; Castano, V. Studies on the precipitation behaviour of calcium phosphate solutions. *J. Ceram. Process. Res.* **2012**, *13* (1), 5–10.
- (99) Liu, G.; Talley, J. W.; Na, C.; Larson, S. L.; Wolfe, L. G. Copper doping improves hydroxyapatite sorption for arsenate in simulated groundwaters. *Environ. Sci. Technol.* **2010**, 44 (4), 1366–1372.
- (100) Monma, H.; Kamiya, T. Preparation of hydroxyapatite by the hydrolysis of brushite. *J. Mater. Sci.* **1987**, 22 (12), 4247–4250.
- (101) Pu'ad, N. M.; Haq, R. A.; Noh, H. M.; Abdullah, H.; Idris, M.; Lee, T. Synthesis method of hydroxyapatite: A review. *Mater. Today: Proc.* **2020**, *29*, 233–239, DOI: 10.1016/j.matpr.2020.05.536.
- (102) Chen, J. H.; Wang, Y. J.; Zhou, D. M.; Cui, Y. X.; Wang, S. Q.; Chen, Y. C. Adsorption and desorption of Cu (II), Zn (II), Pb (II), and Cd (II) on the soils amended with nanoscale hydroxyapatite. *Environ. Prog. Sustain.* **2010**, 29 (2), 233–241.
- (103) Al-Ghamdi, H.; El-Nahal, M.; Saleh, I.; Elsafi, M.; Sayyed, M.; Almuqrin, A. H. Determination of 238U and 40K Radionuclide Concentrations in Some Granite Rocks by Gamma Spectroscopy and Energy Dispersive X-ray Analysis. *Materials* 2022, 15 (15), 5130.
- (104) Gezahegne, W. A.; Hennig, C.; Tsushima, S.; Planer-Friedrich, B.; Scheinost, A. C.; Merkel, B. J. EXAFS and DFT investigations of uranyl arsenate complexes in aqueous solution. *Environ. Sci. Technol.* **2012**, *46* (4), 2228–2233.
- (105) Troyer, L. D.; Tang, Y.; Borch, T. Simultaneous reduction of arsenic (V) and uranium (VI) by mackinawite: role of uranyl arsenate precipitate formation. *Environ. Sci. Technol.* **2014**, *48* (24), 14326–14334.
- (106) Mehta, V. S.; Maillot, F.; Wang, Z.; Catalano, J. G.; Giammar, D. E. Effect of co-solutes on the products and solubility of uranium(VI) precipitated with phosphate. *Chem. Geol.* **2014**, *364*, 66–75.
- (107) Gorman-Lewis, D.; Shvareva, T.; Kubatko, K.-A.; Burns, P. C.; Wellman, D. M.; McNamara, B.; Szymanowski, J. E. S.; Navrotsky, A.; Fein, J. B. Thermodynamic properties of autunite, uranyl hydrogen phosphate, and uranyl orthophosphate from solubility and calorimetric measurements. *Environ. Sci. Technol.* **2009**, *43* (19), 7416–7422
- (108) Gustafsson, J. P. Visual Minteq. 3 v. 3, e; Jon Petter Gustafsson at KTH: Stockholm, Sweden, 2012.
- (109) Foster, R. I.; Kim, K.-W.; Lee, K. Uranyl phosphate (MUO_2PO_4 , $M=Na^+$, K^+ , NH_4^+) precipitation for uranium sequestering: formation and physicochemical characterisation. *J. Radioanal. Nucl. Ch.* **2020**, 324 (3), 1265–1273.
- (110) Islam, M.; Patel, R. Synthesis and physicochemical characterization of Zn/Al chloride layered double hydroxide and evaluation of its nitrate removal efficiency. *Desalination* **2010**, 256 (1–3), 120–128.
- (111) Bachmaf, S.; Planer-Friedrich, B.; Merkel, B. J. Effect of sulfate, carbonate, and phosphate on the uranium (VI) sorption behavior onto bentonite. *Radiochim. Acta* **2008**, *96* (6), 359–366.